nature climate change

Supplementary information

https://doi.org/10.1038/s41558-025-02397-9

Shifting hotspot of tropical cyclone clusters in a warming climate

In the format provided by the authors and unedited

Table of Content:

Supplementary Figures

Supplementary Tables

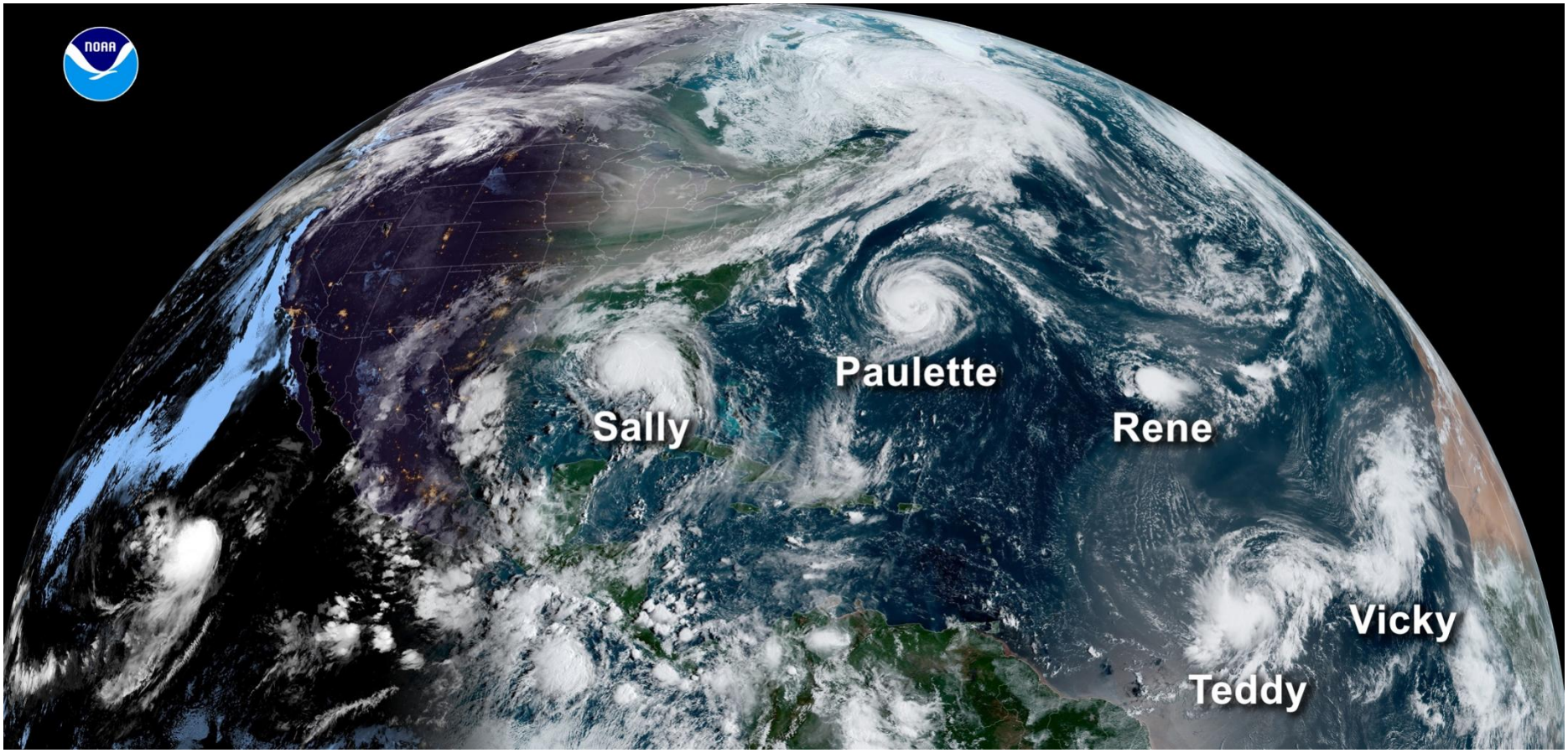

Supplementary Fig. 1 | Five tropical systems spinning in the Atlantic basin at one time. This image is from NOAA's GOES-16 satellite on September 14, 2020. From left to right: Hurricane Sally in the Gulf of Mexico, Hurricane Paulette east of the Carolinas, the remnants of Tropical Storm Rene in the central Atlantic, and Tropical Storms Teddy and Vicky in the eastern Atlantic. A total of 10 named storms formed in September 2020 — the most for any month on record. (Image credit: NOAA).

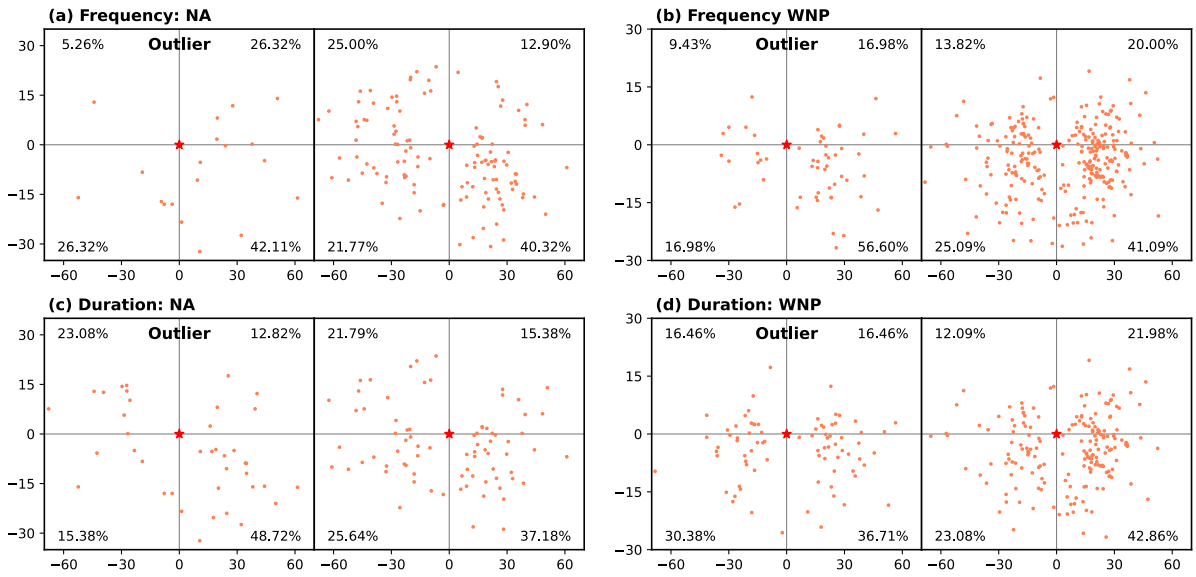

Supplementary Fig. 2 | Identification of dynamically connected TC clusters in observations. a, b, Relative locations between pre-existing TCs (red star) and subsequent TCs (orange dots) at the cyclogenesis time of the subsequent TCs in the outlier group (left) and normal group (right) categorized by TC cluster frequency in the NA (**a**) and WNP (**b**) based on observations during 1979–2014. **c, d,** Same as in **a, b** but categorized by TC cluster duration. Percentages of subsequent TCs in each quadrant are indicated in the four corners.

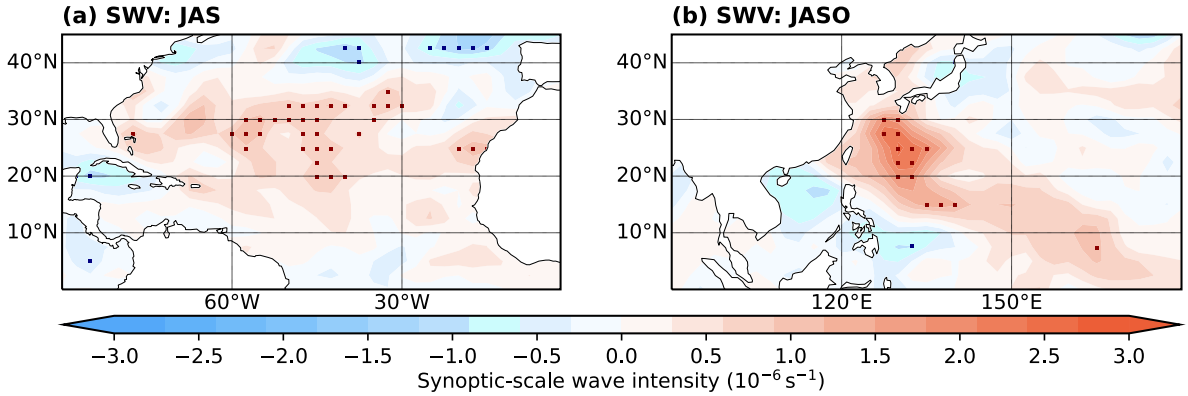

Supplementary Fig. 3 | Synoptic-scale wave intensity changes associated with TC dynamic connections in TC clusters based on NCEP/DOE Reanalysis II. a, b, Composite differences in synoptic-scale wave intensity (10^{-6} s^{-1}) between the two groups bounded by the 50th percentile of TC cluster frequency in probabilistic simulations during 1979–2020 in the NA (**a**) and WNP (**b**). Averages of changes are shown for TC peak seasons in each basin (i.e., JAS for the NA and JASO for the WNP). Dots indicate statistically significant differences at a 95% confidence interval based on the 1000-sample bootstrapping and false discovery rate test. Basemaps from Natural Earth (https://www.naturalearthdata.com).

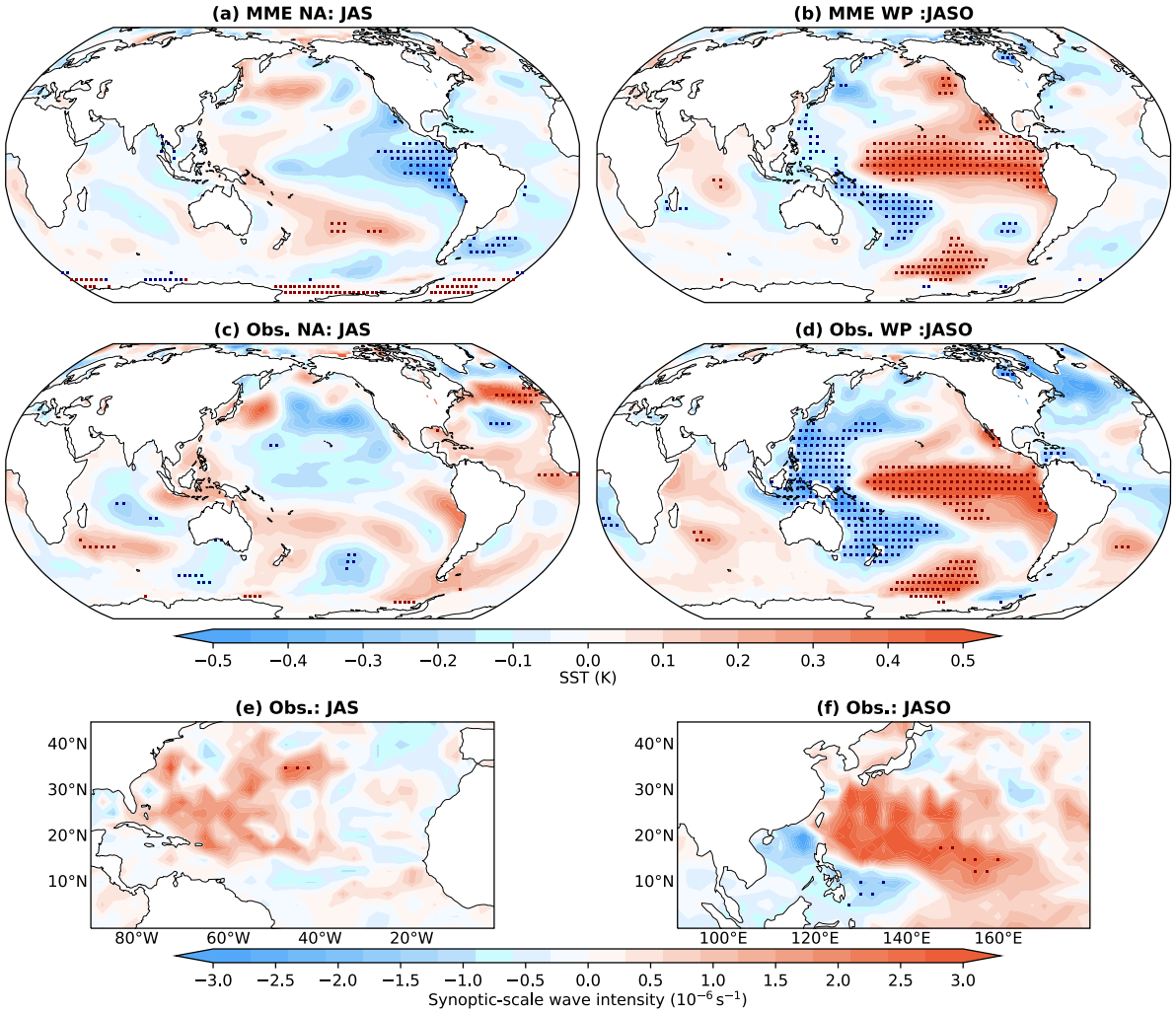

Supplementary Fig. 4 | Patterns of SST and synoptic-scale wave activity that are favorable for dynamically connected TC clusters based on their durations. a, b, Composite differences in SST (K) between TC cluster outlier group and normal group during 1950–2014 based on the MME of the highresSST-present simulations from CMIP6-HighResMIP. To isolate the dynamically connected TC clusters from randomly generated events, the normal and outlier groups are categorized by the 15th and 95th percentile of TC cluster frequency based on the probabilistic modeling in the NA (**a**) and WNP (**b**) (Methods). **c, d,** Same as in **a, b** but for observations with two groups divided by 50th percentile of TC cluster frequency during 1979–2024, to ensure a sufficient and comparable sample size for the two groups. **e, f,** Same as in **c, d** but for differences in synoptic-scale wave intensity (10^{-6} s^{-1}) over the NA (**e**) and WNP (**f**). Averages of changes are shown for TC peak seasons in each basin (i.e., JAS for the NA and JASO for the WNP). In all panels, the dots indicate statistically significant differences at a 95% confidence interval based on the 1000-sample bootstrapping and false discovery rate test. Basemaps from Natural Earth (https://www.naturalearthdata.com).

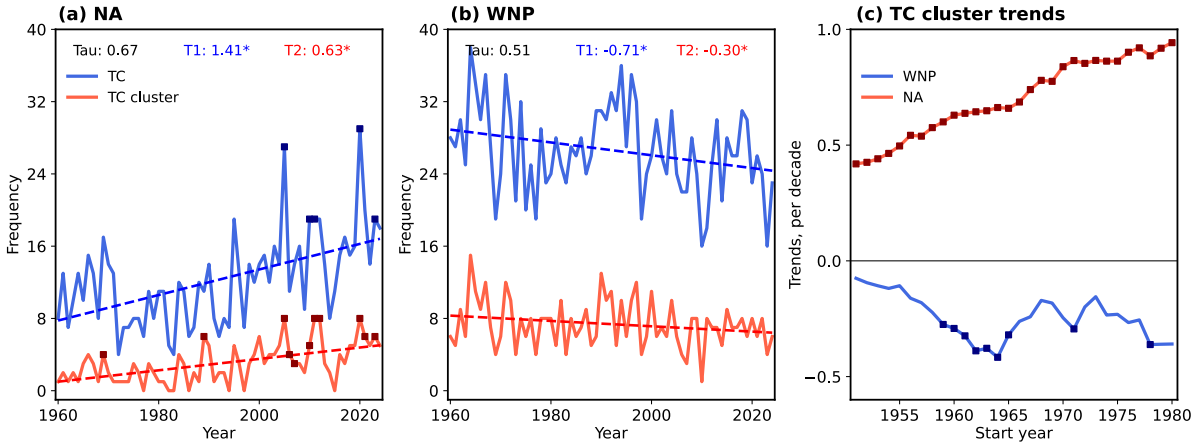

Supplementary Fig. 5 | Sensitivity tests with extended TC dataset. Time series of TC frequency (blue lines) and TC cluster frequency (orange lines) during 1960–2024 over the NA (**a**) and WNP (**b**). Linear trends of TC cluster frequency over the NA (red line) and WNP (blue line), calculated for different start years up to 2024 (**c**). In **a**, **b**, Kendall rank correlations (Tau) between TC frequency and TC cluster frequency are shown at the upper left. The linear trends of TC frequency (T1) and TC cluster frequency (T2) are plotted as dotted lines, with the associated 10-year trend values presented in the upper panel. Asterisks denote significance at the 95% confidence level based on the 1000-sample bootstrapping. Bold dots in **a** indicate that the frequency over the NA reaches or exceeds that over the WNP during 1960–2024. In **c**, red and blue dots denote significant trends at the 95% confidence level through 1000-sample bootstrapping for the NA and WNP, respectively.

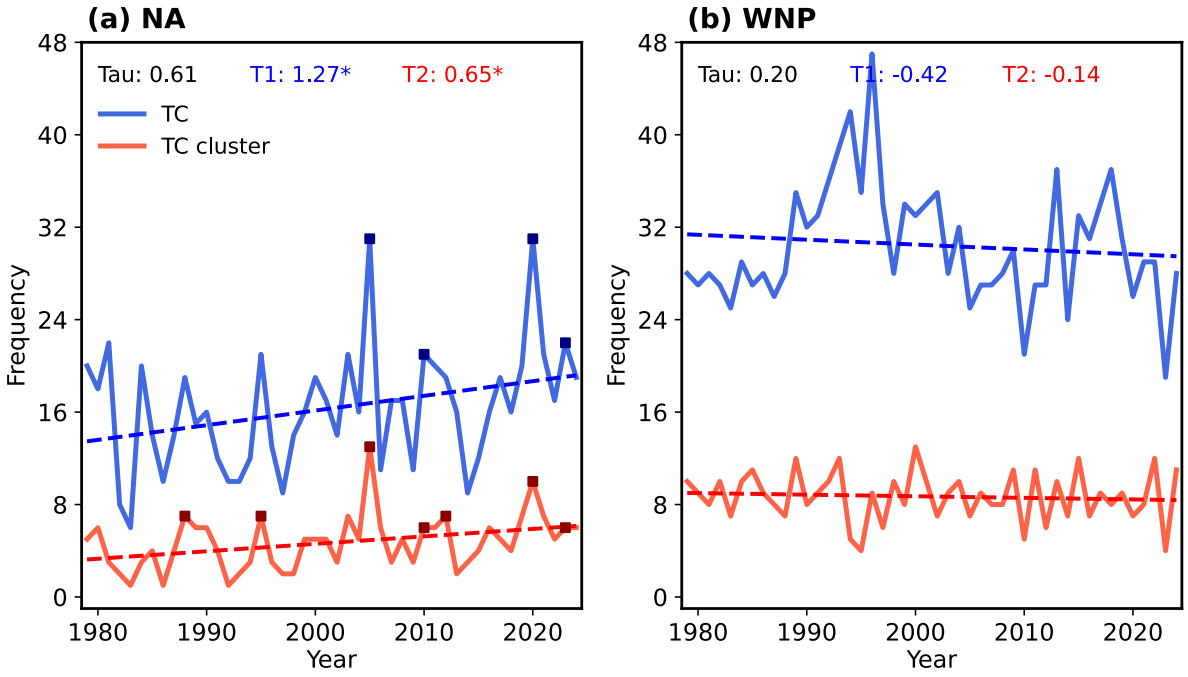

Supplementary Fig. 6 | Sensitivity tests based on different TC detection standards. Time series of TC frequency (blue lines) and TC cluster frequency (orange lines) during 1979–2024 over the NA (**a**) and WNP (**b**), when tropical depressions, extratropical cyclones, and subtropical storms are included. In **a**, **b**, Kendall rank correlations (Tau) between TC frequency and TC cluster frequency are shown at the upper left. The linear trends of TC frequency (T1) and TC cluster frequency (T2) are plotted as dotted lines, with the associated 10-year trend values presented in the upper panel. Asterisks denote significance at the 95% confidence level based on the 1000-sample bootstrapping. Bold dots in **a** indicate that the frequency over the NA reaches or exceeds that over the WNP during 1979–2024.

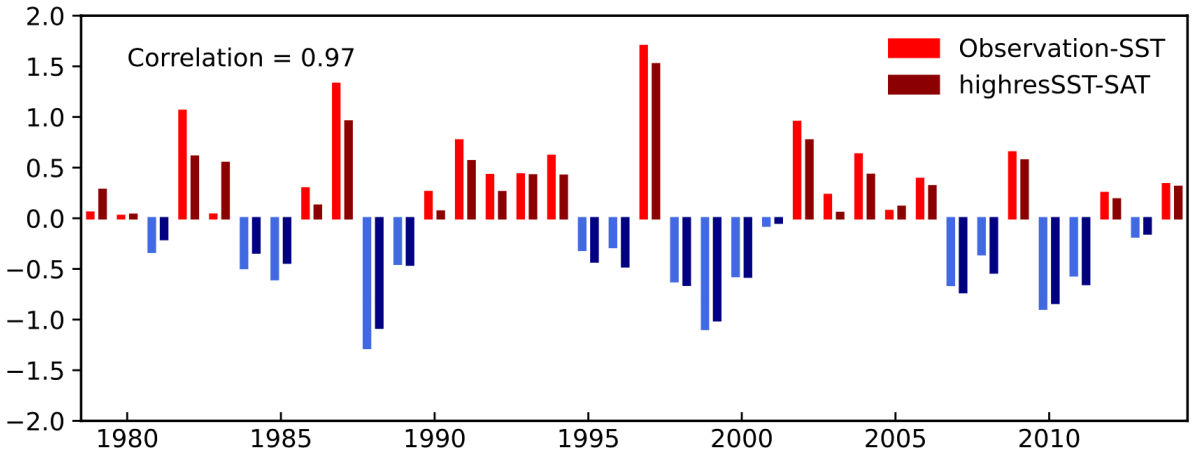

Supplementary Fig. 7 | Validation of SAT as a substitute for SST. Time series of the Niño3.4 index based on observed SST (dark histogram) and SAT in CMIP6-HighResMIP simulations (light histogram) during 1979–2014. The correlation between the two time series reaches 0.97 during 1979–2014, indicating that SAT is highly consistent with SST. Red/blue indicate that the index is above/below zero.

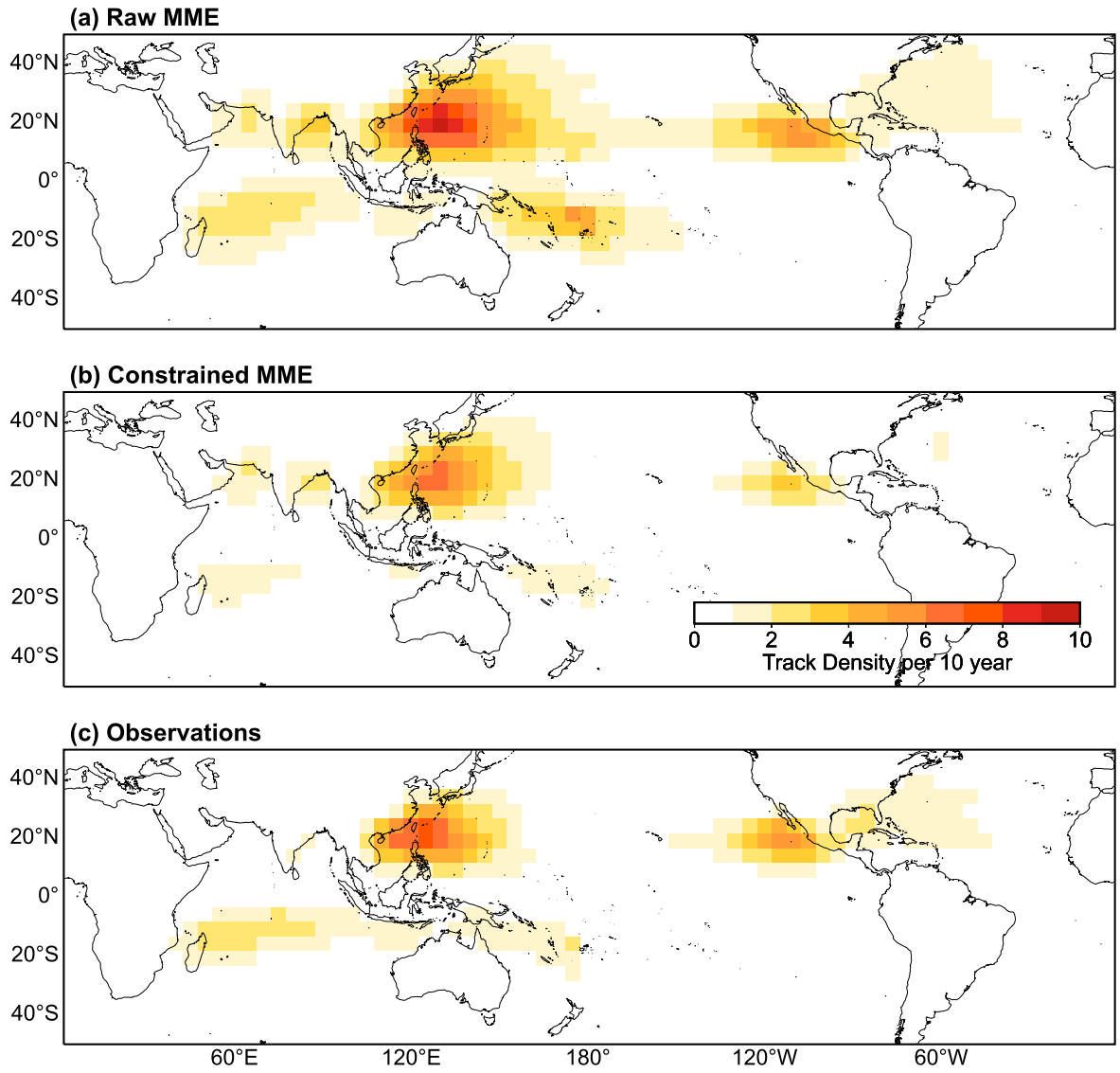

Supplementary Fig. 8 | Comparison of simulated and observed TC track density. a, Global distribution of TC track density in the MME of the highresSST-present simulations from CMIP6-HighResMIP during 1979–2014 without constraints. **b,** Same as in **a** but for constrained MME. **c,** Same as in **a** but for observations. Basemaps from Natural Earth (https://www.naturalearthdata.com).

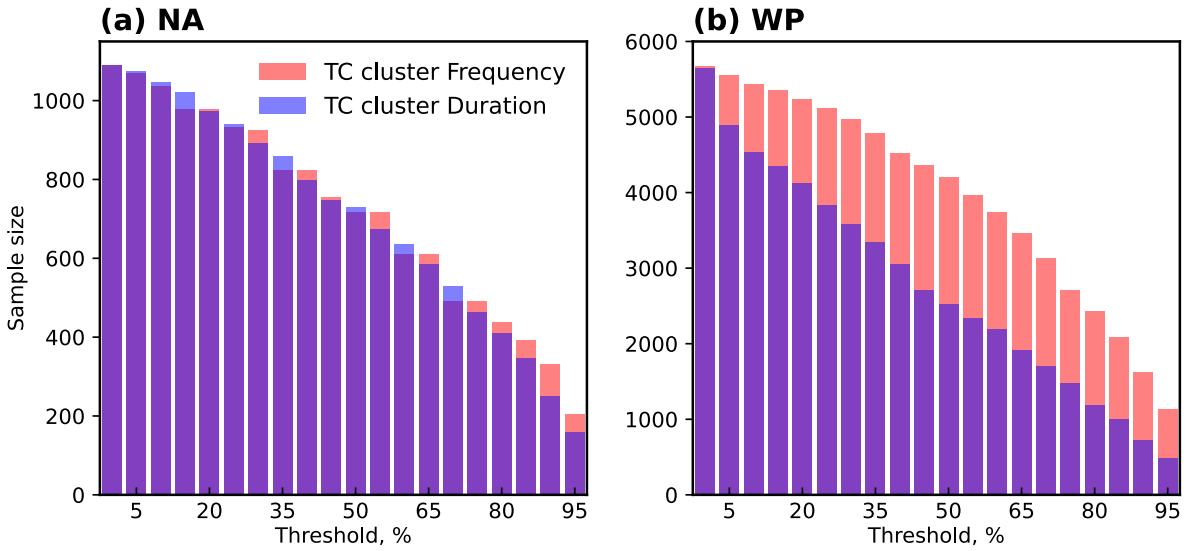

Supplementary Fig. 9 | Sample size for threshold test analysis. a, b, Total counts of subsequent TCs with different threshold definition for outliers categorized by TC cluster frequency (red histogram) and TC cluster duration (blue histogram) in the NA (**a**) and WNP (**b**).

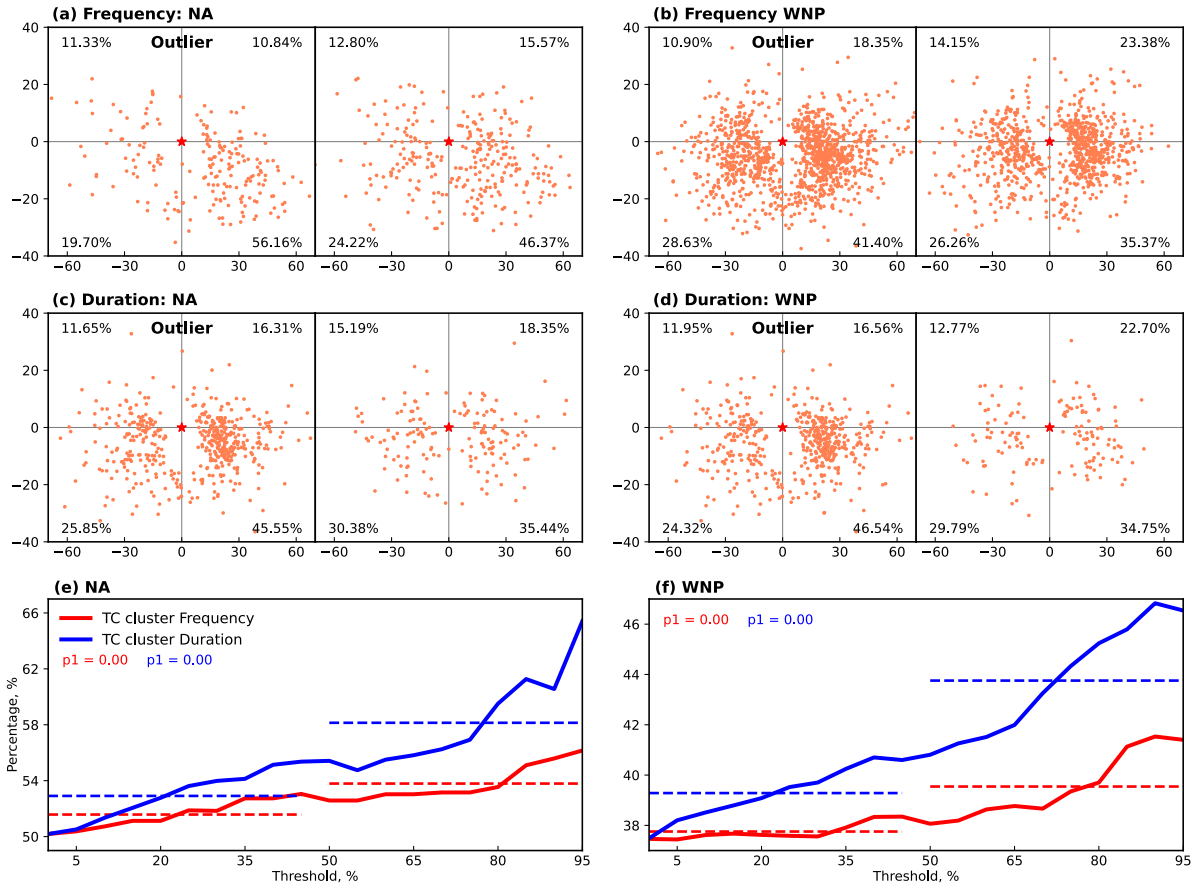

Supplementary Fig. 10 | Identification of dynamically connected TC clusters without a distance constraint. a, b, Relative locations between pre-existing TCs (red star) and subsequent TCs (orange dots) at the cyclogenesis time of the subsequent TCs in the outlier group (left) and normal group (right) categorized by TC cluster frequency in the NA (**a**) and WNP (**b**) based on the MME of the highresSST-present simulation in seven high-resolution climate models from CMIP6-HighResMIP during 1950–2014. **c, d,** Same as in **a,b** but categorized by TC cluster duration. Percentages of subsequent TCs in each quadrant are indicated in the four corners. **e, f,** Percentages of subsequent TCs located in the southeastern quadrant with different percentile thresholds to define the outlier group in the NA (**e**) and WNP (**f**), categorized by TC cluster frequency (red lines) and TC cluster duration (blue lines) (Methods). The average ratios between the two regimes, separated by a threshold of 50%, are plotted as dotted lines. The mean ratios between the two stages are statistically different with p-values less than 0.01 based on the 1000-sample bootstrapping.

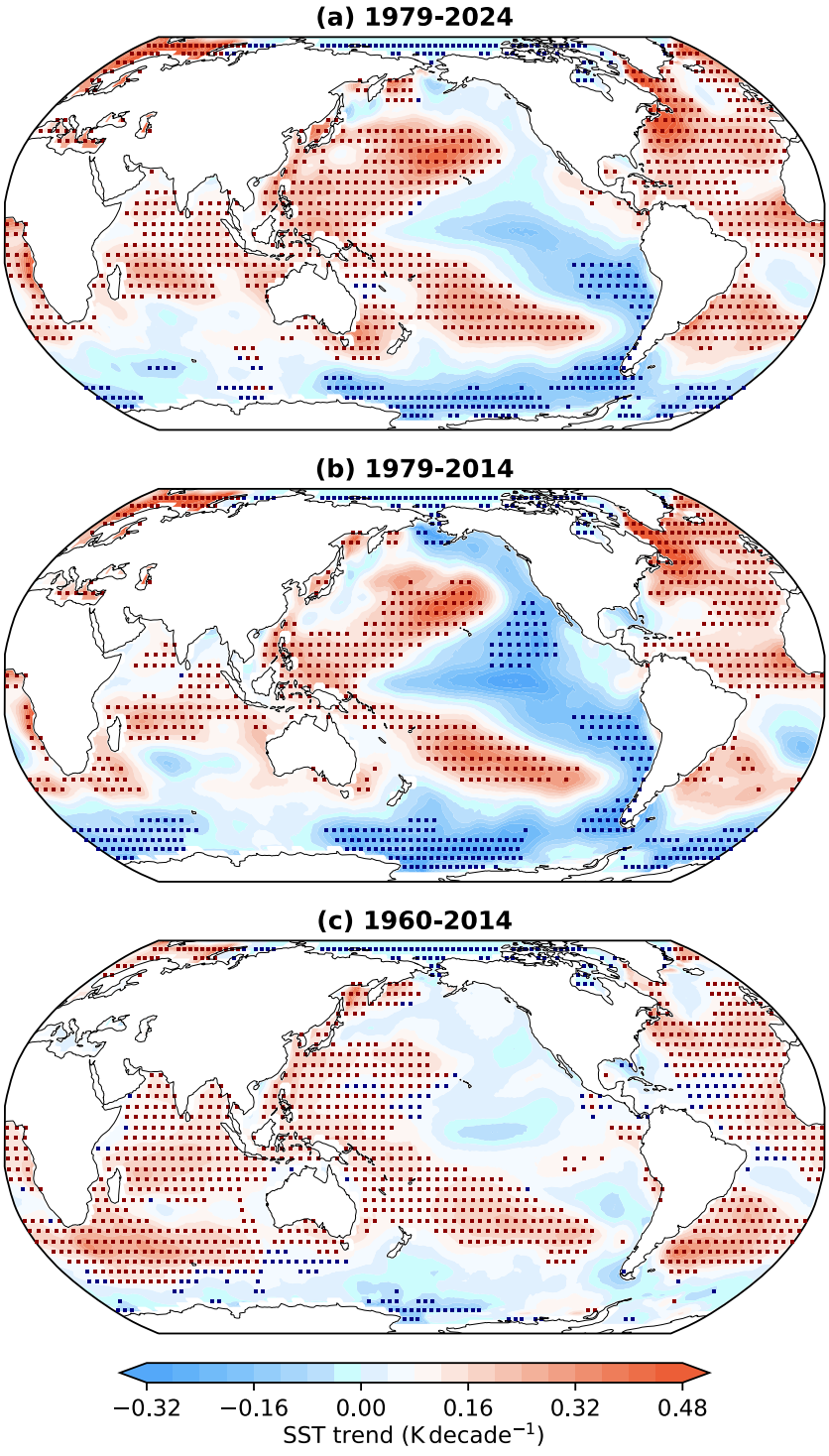

Supplementary Fig. 11 | Observed surface warming patterns over different periods. a-c, Linear trends of global SST (K decade^{-1}) during 1979–2024 (**a**), 1979–2014 (**b**), and 1960–2014 (**c**). To highlight relative warming patterns, the color scale is centered on the mean tropical warming rate (about 0.08 K decade^{-1}). Dotted areas indicate 95% significance, determined using 1000-sample bootstrapping and false discovery rate test. Basemaps from Natural Earth (https://www.naturalearthdata.com).

Supplementary Table 1 | TC cluster changes in the seven individual models and MME from CMIP6-HighResMIP during the periods 1981–2010 and 2020–2049. Statistically significant changes at the 95% confidence interval based on the 1000-sample bootstrapping are bolded.

Model	NA		WNP	
	Frequency	Duration	Frequency	Duration
CNRM	**0.77**	**3.93**	**-2.97**	**-13.43**
EC-Earth	0.67	1.07	**-2.47**	**-12.13**
HadGEM	0.43	1.33	**-1.57**	**-6.07**
MRI-S	0.03	**5.80**	**-2.43**	**-14.77**
MRI-H	**0.60**	2.17	**-1.77**	**-10.77**
NICAM-8S	**1.27**	**5.00**	**-3.10**	**-13.67**
NICAM-7S	0.37	1.37	**-3.12**	**-12.80**
MME	**0.59**	**2.95**	**-2.50**	**-11.95**

Supplementary Table 2 | The CMIP6-HighResMIP models, including their resolutions, references, and constraint detection thresholds.

Model	Description		Constraint Detection Threshold		
	Resolution	Reference	Wind speed	Duration	SST
CNRM-CM6-1-HR	50 km	Voldoire et al., (2019) (ref. [54])	16 m/s	12 hours	26 ℃
EC-Earth3P-HR	50 km	Haarsma et al. (2020) (ref. [55])	11 m/s	-	26 ℃
HadGEM3-GC31-HM	50 km	Roberts et al. (2019) (ref. [56])	20 m/s	12 hours	26 ℃
MRI-AGCM3-2-S	20 km	Mizuta et al. (2022) (ref. [57])	13 m/s	-	26 ℃
MRI-AGCM3-2-H	60 km	Mizuta et al. (2022) (ref. [57])	13 m/s	-	26 ℃
NICAM16-8S	28 km	Kodama et al. (2021) (ref. [58])	31 m/s	24 hours	26 ℃
NICAM16-7S	56 km	Kodama et al. (2021) (ref. [58])	33 m/s	24 hours	26 ℃

Supplementary Table 3 | Comparison of simulated and observed basin-wide frequencies and their standard deviations in six basins during 1979–2014.

	Observations	Constraint MME	Raw MME
NA	12.0 ± 4.8	6.9 ± 3.4	16.4 ± 12.6
WP	26.4 ± 4.5	27.0 ± 7.7	42.1 ± 22.1
EP	16.5 ± 4.5	11.0 ± 5.4	26.5 ± 21.4
NI	5.1 ± 1.8	7.4 ± 3.9	10.7 ± 6.2
SI	18.6 ± 3.5	13.5 ± 5.2	22.8 ± 11.5
SP	11.4 ± 4.5	12.6 ± 5.0	33.7 ± 21.5